Catalysis Today 136 (2008) 281–290

Contents lists available at ScienceDirect

Catalysis Today

journal homepage: www.elsevier.com/locate/cattod

Hydrogen generation by catalytic gasification of motor oils in an integrated fuel processor

Kuen-Song Lin *, Sujan Chowdhury, Chia-Chieh Shen, Chuin-Tih Yeh

Department of Chemical Engineering and Materials Science/Fuel Cell Center, Yuan Ze University, 135 Yuan-Tong Road, Chung-Li City, Tao-Yuan County 32061, Taiwan, ROC

ARTICLE INFO

Article history:
Available online 21 April 2008

Keywords:
Waste motor oil
Catalytic gasification
Reforming
Hydrogen generation
Fuel processor
Syngas

ABSTRACT

Catalytic gasification of waste motor oil (MO) for the generation of high purity of hydrogen and then integrated to a proton exchange membrane fuel cell (PEMFC) is economically and environmentally attractive. Thus, the objective of the present work was to investigate a MO catalytic gasification for generating high-purity hydrogen with 15 wt.% NiO/Al_2O_3 catalysts. In a lab-scale fixed-bed downdraft experimental approach, catalytic gasification of MO was accompanied by a substantial production of syngas at 760–900 K. From the XANES spectra, most of the Ni(II) reduced to Ni(0) was found in the MO catalytic gasification process. The EXAFS data also showed that the central Ni atoms have a Ni–O and a Ni–Ni with bond distances of 2.04 ± 0.05 Å and 2.48 ± 0.05 Å, respectively. In addition to over 85% of syngas generation, approximately 8.35×10^5 kcal h^{-1} of thermal energy was recovered and cold gas efficiency (CGE) was 77–84% when the catalytic gasifier was operated at O/C atomic ratios between 1.1 and 1.3. The proposed syngas production unit can be integrated in a fuel processor (e.g. PEMFC), in order to separate and purify the syngas to yield a 99.99% hydrogen stream. Moreover, cost or benefit analyses of MO catalytic gasifiers of 10- and 20-TPD (tons per day) were also performed.

1. Introduction

Over 600,000 tons per year (TPY) of waste liquid oils such as waste MO, were produced in Taiwan in the last decade [1]. These waste MOs are the major liquid in car maintenance or repair shops and abundantly available in the city or countryside. Improper disposal of MO could cause negative environmental impact in the end. However, MOs have been considered a recoverable waste, causing disposal and disease problem. Like most other organic materials, MOs contain a high amount of organic volatiles [2–5]. Thus, steam reforming or gasification of MO has been known as one of effective technology options for the utilization of renewable hydrogen energy resources [6–8]. Hydrogen, a clean and new energy carrier for the future, is usually generated by chemical conversion of fuels such as MO, hydrocarbons or organics [9,10]. In addition, the effective and active catalysts in reforming MOs have the advantages of resisting carbon attrition and deactivation [11–13]. The main challenges of implementing and improving catalytic reforming technology are to develop a suitable catalyst for enhancing the tar/char, NH_3 or H_2S removal and therefore increasing synthesis gas (syngas, $CO + H_2$) yield, separating or purifying the product gases, and then high-purity hydrogen generated for a PEMFC system. Catalytic gasification of waste MOs to produce synthesis gas and heat energy may be an appealing resource recovery alternative. In a catalytic gasification process, the hazardous waste MOs, which can be accepted as a feedstock without any pretreatment, are partially oxidized under chemically reducing atmosphere in the gasifier and ultimately converted into CO and H_2. In such a process, the destruction and removal efficiency (DRE) was high and no or trace toxic by-products (such as polychlorinated dibenzo-*p*-dioxins and dibenzofurans (PCDDs/DFs) or polycyclic aromatic hydrocarbons (PAHs) were formed [5–9]. On the other hand, a small amount of NO_x or SO_x was generated and an air pollution control device (APCD) (such as selective catalytic reduction unit on a stack) is not required. Since the catalytic gasification of waste MO takes the above-mentioned benefits, it has become an innocent and economically advantageous strategy for waste MOs decomposition.

In previous works, some catalytic systems have been investigated including metal oxides, active metals or cheap minerals [14–23]. Comparatively, the best activity, short contact time, high conversion ratio or inexpensive of nickel catalysts supported on zeolites, Al_2O_3 or CeO_2 were found [24–33]. Nickel catalyst is the well-known attractive catalyst among metals like Co, Fe, Pt, Ru or Rh due to the performance and economical reason [14,34]. However, nickel catalyst can be used effectively after reducing the catalyst deactivation and erosion problem. Catalyst deactivation is occurred due to the carbon (coke) fouling and sintering

* Corresponding author. Tel.: +886 34638800x2574; fax: +886 34559373.
E-mail address: kslin@saturn.yzu.edu.tw (K.-S. Lin).

0920-5861/$ – see front matter © 2008 Elsevier B.V. All rights reserved.
doi:10.1016/j.cattod.2008.02.017

effects on the catalyst surface. Stronger interaction between NiO and support can restrain the loss and sintering of nickel [35–37]. To develop more stable catalysts, alumina-based material can be act as a primary support for decrease the catalyst deactivation. Nickel-based catalyst is also deactivate due to the catalytic poisoning. Strong chemisorptions of impurities (mainly H_2S or SO_x) are occurred onto the catalyst active sites and then deactivate the catalyst [38]. Forzatti and Lietti [39] reported that sulfur adsorption decreases with increasing temperature and conditioning the feed gas to the catalyst can prevent poisoning and significantly increased gas formation. Therefore, development of more effective gasification methods based on highly active nickel catalysts has been paid great attention because it cannot only gasify the organic compounds but also recover hydrogen or CO in syngas [33–39].

Recently, hydrogen production process is applied effectively for environmental impact and energy generation issues. A PEMFC utilizing H_2 as a fuel would produce almost negligible amount of pollutants. Generally, a PEMFC system includes three major parts such as PEMFC processor, PEMFC stack and power conditioner [6,40,41]. A fuel processing is defined as conversion of any hydrocarbons or organics to a fuel gas and this reformation is suitable for PEMFC anode reaction system [40–43]. In an integrated PEMFC, waste MO can be processed to produce H_2-rich syngas through several steps including reforming, steam reforming or water gas shift reaction, and preferential oxidation. Furthermore, H_2/oxygen (or air) mixture is fed to the PEMFC stack for a direct electric current generation and then is converted to an alternating electric current by the power conditioner [42–44]. Reforming process of waste MO is one of the potential organic sources of hydrogen and generates heat energy. The high purity of hydrogen fed to the PEMFC stack for power generation makes waste MO utilization system economically and environmentally attractive.

Therefore, the main objectives of the present work were to assess the feasibility of waste MO catalytic gasification with syngas recycling for the potential application on an integrated fuel processor (e.g. PEMFC) system. Lab-scale waste MO catalytic gasification experiments were conducted in the present study to ensure an operationally simple and economically attractive process developed. The physicochemical properties, morphology and fine structures of fresh and waste MO, product gases or 10–15 wt.% NiO/Al_2O_3 catalysts were also further measured and identified by elemental analyzer (EA), gas chromatography (GC), thermogravimetric analyzer (TGA), transmission electron microscopy (TEM), field emission-scanning electron microscopy (FE-SEM), Fourier transform infrared spectroscopy (FTIR) or X-ray absorption near edge structural (XANES)/extended X-ray absorption fine structural (EXAFS) spectroscopies. In addition, cost or benefit analysis of waste MO catalytic gasification was also performed to confirm the economic potential for such a recycling practice and determine if further developments would be warranted.

2. Experimental

2.1. Catalyst preparation

The 10–15 wt.% NiO/Al_2O_3 catalysts were prepared by impregnation method of high surface area alumina with an excess of nickel nitrate solution. About 10 g support of well-milled Al_2O_3 ultrafine particles were mixed with 7–10 g $Ni(NO_3)_2{\cdot}6H_2O$ in 30 mL water solution. After water evaporation, the solid residues were calcined under a flowing air for 5–8 h at 1273 K. In addition, the Ni concentrations of as-synthesized catalysts were also identified and calculated using atomic adsorption spectroscopy (AAS, PerkinElmer AA200) and inductively coupled plasma-optical emission spectroscopy (ICP-OES, PerkinElmer Optima 2100DV).

2.2. Lab-scale MO catalytic gasifier

In order to obtain the basic data for development of the waste MO catalytic gasification process, catalytic reforming tests of waste MO were conducted in a lab-scale downdraft type reactor. Experiments of waste MO catalytic gasification were performed in a continuous-flow/fixed-bed reactor enclosed in electrically heated jackets and operated under isothermal and isobaric conditions. Owing to improve the well temperature distribution and lower pressure drop in the catalytic gasifier, about weight ratio of catalyst/quartz chips (1–2-mm size) = 2/5 was held between the quartz wool plugs placed at the center of the waste MO catalytic gasifier. A schematic diagram of waste MO catalytic gasification system at 760–900 K and 1 atm was shown in Fig. 1. The catalytic gasifier was a stainless steel tube with 2.54-cm i.d. and 60-cm long. All parts and connections used in the gasifier were brass or stainless steel, and the gas inlet and outlet flow systems were well-sealed polyethylene tubes. Catalytic gasification of waste MO (Shell 20W-50 motor oil (MO) with a flow rate of 50 mL h^{-1}) was conducted at 760–900 K (average operating temperature of 830 K) with a mixing flow of 10.5–21.0 vol.% O_2 and steam (gas hourly space velocity (GHSV) = 1200 h^{-1} at STP) and improved by operating the gasifier at O/C atomic ratios between 1.10 and 1.30. In addition, the durability of all the NiO/Al_2O_3 catalysts for

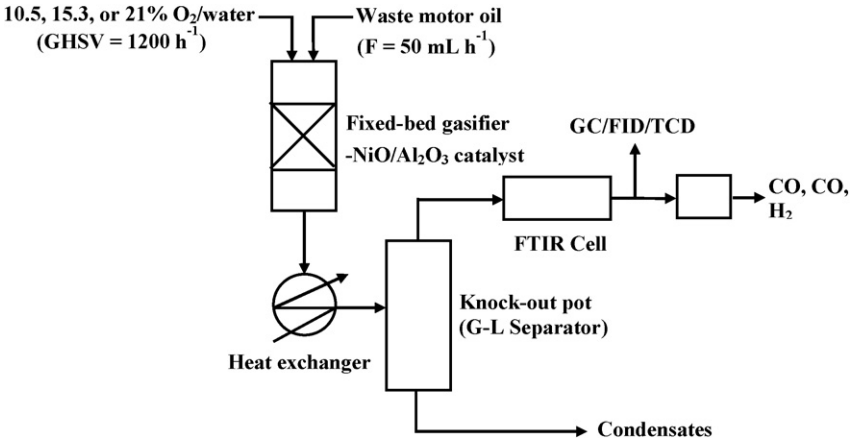

Fig. 1. A schematic flow diagram of a lab-scale catalytic gasification system for waste MO on 15 wt.% NiO/Al_2O_3 catalyst at 760–900 K and 1 atm.

MO gasification was 10 h and the used catalysts were also further identified using XRD, FE-SEM or TEM techniques. All reagents used were ACS grade and the purity of these reagents was >99%. Noncondensible gases generated in the catalytic gasifier were passed through a water cooler and was measured by using a totalizer. The condensates were separated and collected in the two knockout drums (500 mL and 300 mL, in series). The noncondensible gases were sampled and analyzed by an *on-line* FTIR spectroscope and then scrubbed with 1 M NaOH solutions before emitting.

2.3. Thermogravimetric analyses and kinetics of MO

Preliminary studies and basic engineering design of catalytic gasification of MO with 15 wt.% NiO/Al_2O_3 catalyst (catalyst/MO wt. ratio = 5 and molar steam-to-oxygen-to-carbon ratio (S/O/C) = 1.5/1.1/1.0) were investigated using a TGA (model SDT 2960 & Thermal Analyst 2000, TA Instruments). Reaction temperatures and MO/catalyst sample weights were recorded at 10-s intervals. About 30 mg of samples were heated from 303 K to 823 K at a heating rate of 5 K min^{-1}, 10 K min^{-1} or 15 K min^{-1} with a sensitivity of 0.1 ± 0.01 μg in a mixing flow of 10.5–21.0 vol.% O_2 and steam (100 mL min^{-1}) in the TGA. The calibration procedures were performed once a month, including TGA weight calibration, differential thermal analysis (DTA) baseline calibration and temperature calibration. In all experiments, aluminum oxide was used as a reference. Gasification kinetic parameters derived from the TGA data (such as activation energy and pre-exponential factor) were based on the classical laws of kinetics. Detailed descriptions of the method have been given by Petrović and Zavargo [45] and Friedman [46] covered important techniques for evaluating the kinetic parameters from the TGA traces. The overall rate equation of conversion factor expressed in the Arrhenius relation form for catalytic gasification reaction is as following:

$$\ln\left(\frac{dX}{dt}\right) = \ln\ A_p + n\ \ln(1-X) + \left(\frac{-E_a}{RT}\right) + m\ \ln[O_2]$$

$$X = \frac{W_0 - W}{W_0 - W_f}, \qquad k = A_p\ \exp\left(\frac{-E_a}{RT}\right)$$

where t is the reaction time (min), A_p is the pre-exponential factor (min^{-1}), E_a is the activation energy (kcal mol^{-1}), k is the Arrhenius rate constant, T is the reaction temperature (K), R is universal gas constant (1.987×10^{-3} kcal g mol^{-1} K^{-1}), W is the mass of the sample at time t, $g(O_2)$ is the mth order for the oxygen composition, $f(X)$ is the nth order for the unreacted MO, and W_0 and W_f are the initial and final (or residual) mass of the samples, respectively.

2.4. Characterization methods of waste MO and catalysts

Proximate and ultimate analyses of waste MO composition were performed in the initial stage using traditional EA (EA, F002-heraeus rapid CHN–O) as a tool. The results of elemental analyses of fresh and waste MOs are shown in Table 1, in which combustible content constitutes the main component of a typical fresh or waste MO mixture obviously. The compositions of gas products for waste MO catalytic gasification, such as a syngas ($CO + H_2$), were also analyzed by using GC (Agilent, 6890N) and FTIR spectroscopy (10-cm gas cell). Infrared spectra were recorded on a Digilab FTIR spectrometer (FTS-40) with fully computerized data storage and data handling capability. For all spectra reported, a 64-scan data accumulation was conducted at a resolution of 4 cm^{-1}.

Morphologies and microstructures of NiO/Al_2O_3 catalyst samples were determined by FE-SEM/EDS (Hitachi, S-4700 Type II). TEM analyses were conducted to investigate the crystallinity and particle size distribution of the catalyst samples with a Model Zeiss 10C using 150 kV accelerating voltage. Crystalline phase or structures of Ni, NiO standards or NiO/Al_2O_3 catalysts were measured by XRD scanned from 15° to 90° (2θ) with a scan rate of 4° (2θ)/min with monochromatic Cu Kα radiation (MAC Science, MXP18). The BET surface area of NiO/Al_2O_3 catalysts for waste MO gasification was obtained from the conventional analysis of nitrogen isotherms measured at 77 K with Micrometrics TriStar 3000 apparatus. All the catalyst samples were degassed at 100 °C prior to the measurement. The surface area of the as-synthesized 10–15 wt.% NiO/Al_2O_3 catalysts is ranged from 125 m^2 g^{-1} to 150 m^2 g^{-1}.

XANES/EXAFS spectra of nickel catalysts were collected at Wiggler 17C1 beamline of Taiwan National Synchrotron Radiation Research Center (NSRRC). The electron storage ring was operated with the energy of 1.5 GeV and a current of 100–200 mA. A Si(1 1 1) DCM was used for providing highly monochromatized photon beams with energies of 1–15 keV and resolving power of up to 7000. Data were collected in fluorescence or transmission mode with a Lytle ionization detector [47] for Ni (8333 eV) K edge experiments at room temperature. Characteristic pre-edge peaks in the absorption spectra of Ni standards calibrated photon energy. Raw absorption data in the region of 50–200 eV below the edge position were fit to a straight line using the least-square algorithms. The fitted pre-edge background curves were extrapolated throughout all data range, and subtracted and normalized to minimize the effect of catalyst sample thickness. Near-edge structure in an absorption spectrum covers the range between the threshold and the point at which the Ni EXAFS begins. The Ni XANES extend to the energy of the order of 50 eV above the edge. The k^3-weighted and EXAFS spectra were Fourier transformed to R space over the range of 2.5–12.5 $^{-1}$. Ni EXAFS data were analyzed by UWXAFS 3.0 program and FEFF 8.0 codes.

Table 1
Proximate and ultimate analyses of typical fresh and used motor oils in Taiwan

	Fresh MO	Used MO
Proximate analysis (wt.%)		
Combustibles	99.28	97.92
Moisture	0.34	0.62
Ash	0.38	1.46
Ultimate analysis (wt.%)		
Carbon	84.80	81.72
Hydrogen	13.19	13.28
Nitrogen	0.92	1.02
Sulfur	1.03	0.56
Chlorine	Not detectable	0.05
Oxygen	Balanced	Balanced
High heating value (kcal kg^{-1})	13,450	12,830

3. Results and discussion

3.1. Proximate, ultimate and kinetics analyses of MO

The combustible content constitutes the main component of a typical fresh or a waste MO is shown obviously in Table 1. Since the cracking of aliphatics or paraffins caused by thermal or pressure stress of engine for a car or a motorcycle then trace metal powder or carbon black is contaminated in waste MO. It can be seen that the compositions of both fresh and waste MOs are different especially for the concentration of ash, moisture or chlorine species. It was also found that the concentration of sulfur in waste MO decreases might be reduced by the heat evaporation of the fresh MO in thermal stress of engines for cars or motorcycles. Typical TGA curves for MO catalytic gasification are shown in Fig. 2.

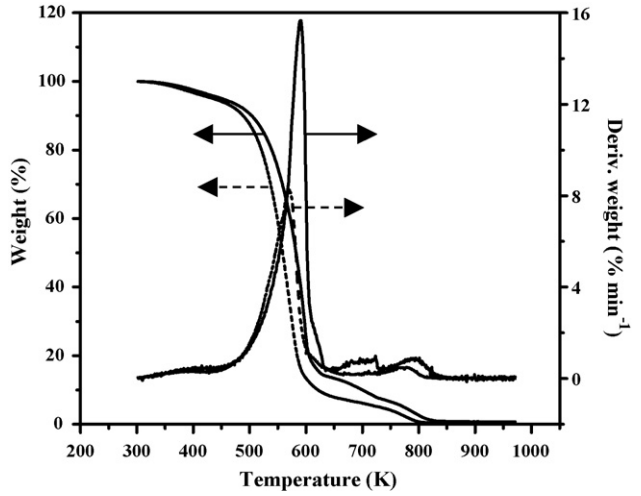

Fig. 2. TGA and DTA curves of fresh (—) and used (– –) MOs with 15 wt.% NiO/Al_2O_3 catalyst (catalyst/MO wt. ratio = 5 and S/O/C = 1.5/1.1/1.0) from 303 K to 823 K at a heating rates of 15 K min^{-1} in a mixing flow of 15.3 vol.% O_2 and steam (100 mL min^{-1}).

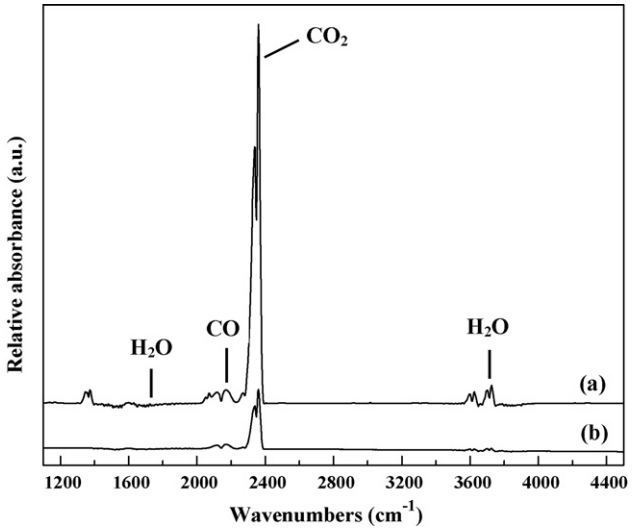

Fig. 3. FTIR spectra of syngas produced from waste MO catalytic gasification (a) with 15 wt.% NiO/Al_2O_3 catalyst and (b) without catalyst at T = 900 K and 1 atm.

Table 2
Kinetic parameters of a lab-scale catalytic gasification system of waste MO for an integrated PEMFC

Carrier gas (vol.% O_2)	E_a (kcal mol^{-1})	ln A_p (min^{-1})	n	m
10.5	21.35	26.41	1.1	0.4
15.3	18.23	23.37	1.2	0.6
21.0	10.53	20.85	1.4	0.7

A two-stage process for thermal degradation of MO is observed. Since the peak of the second-stage was not notably found compared with the first-stage and the approximate postulation of pseudo-first-order catalytic gasification reaction was therefore approached. The derived kinetic parameters of MO obtained from the thermogravimetry experiments are summarized in Table 2. The catalytic gasification of waste MO can be satisfactorily described by the corresponding rate equation.

$$\frac{dX}{dt} = (1.41 \pm 0.50 \times 10^{10})\ \exp((-16.7 \pm 5.5)/(1.987 \times 10^{-3}T)) \times (1-X)^{1.2\pm0.2}[O_2]^{0.6\pm0.2}$$

The conversion and residence time are the main engineering design data used in sizing the reactor as well as optimizing operation conditions. The gasification temperature, on the other hand, is the key factor for determining the desired product distribution. As shown in Fig. 2, it indicates that the distribution of activation energy (E_a) calculated from catalytic gasification kinetics for waste MO was between 10 kcal mol^{-1} and 21 kcal mol^{-1}. The catalytic gasification of MO represents the pseudo-first-order reaction and the oxygen component is in the order of 0.6 ± 0.2. Moreover, the relatively lower activation energy of MO catalytic gasification indicated that this reaction may be easily achieved and the potential of hydrogen generation from MO gasification was observed.

The comparison for typical TGA curves of fresh and waste MOs was shown in Fig. 2. Two main distinct weight loss stages of the waste MO are found. In the first stage, at temperatures around 580 K, high concentrations of gaseous CO_2 and CO are exhausted and also observed by *on-line* FTIR spectroscopy shown in Fig. 3, that may be caused mainly by thermal degradation of fresh or waste MO in the catalytic gasification processes, respectively. Furthermore, in the second-stage catalytic decomposition of fresh or waste MO is occurred due to the depletion of minor and heavier constituents in the temperatures ranged from 750 K to 800 K (Fig. 2). In addition, the peak of maximum degradation temperature of fresh MO is higher and sharper than the one of waste MO. It is also likely that the cracking of aliphatics or paraffins and the formation of olefins for waste MO are observed similarly with Fig. 2 [48,49]. These results are also consistent with the chemical characteristics of fresh and waste MOs for catalytic gasification shown in Table 3.

Proton NMR and FTIR spectroscopies were used to get insight into the structural changes of fresh or waste MOs conditioned by mainly thermal stress or carbon black contamination [48,49]. Table 3 represented that aliphatics (bands with an intense infrared absorbance at 2800–3000 (stretching) and 1375–1450 cm^{-1} (bending)) are the major components in waste MOs. Content of the methyl proton in the aliphatics may be described adequately by the $A_{1380\ cm^{-1}}/A_{2920\ cm^{-1}}$ absorbance ratios (AR). Generally, an increase of the AR value may be attributed to the fact that the cracking of aliphatics or paraffins in waste MO is caused by thermal or pressure stress of engine for a car or a motorcycle. In Table 3, an increase in methyl content of the waste MO compared with the fresh MO is observed. In addition, the derived NMR data using the method in Refs. [49,50] in Table 3 are also suggestive of the occurrence of cyclization in the waste MO since aromatic content in waste MO increases. It is very likely that the aromatics in waste MO may be highly methyl substituted.

3.2. Catalyst characterization

From FE-SEM microphoto, a spherical or irregular shape NiO/Al_2O_3 nanocatalyst included a diameter of approximately 10–20 nm and notably visualized spherical particles are shown in Fig. 4(a). As shown in Fig. 4(c), TEM image also indicated that fresh

Table 3
Chemical characteristics of fresh and waste motor oils for catalytic gasification

	Aromatics[a]	Olefins[a]	Paraffins[a]	Methyl content[b]
Fresh motor oil	4.11	0.76	95.13	18.65
Used motor oil	5.30	11.35	83.35	23.68

Note: results are all normalized to 100% for the summation of aromatics, olefins, and paraffins (unit: vol.%).

[a] Calculated from ^{1}H NMR data using the method in Refs. [49,50].

[b] Methyl content (AR) (H_{CH3} / (H_{CH} + H_{CH2} + H_{CH3})) derived from FTIR spectra using equation: 2.4 ($A_{1380\ cm^{-1}} + A_{2920\ cm^{-1}}$).

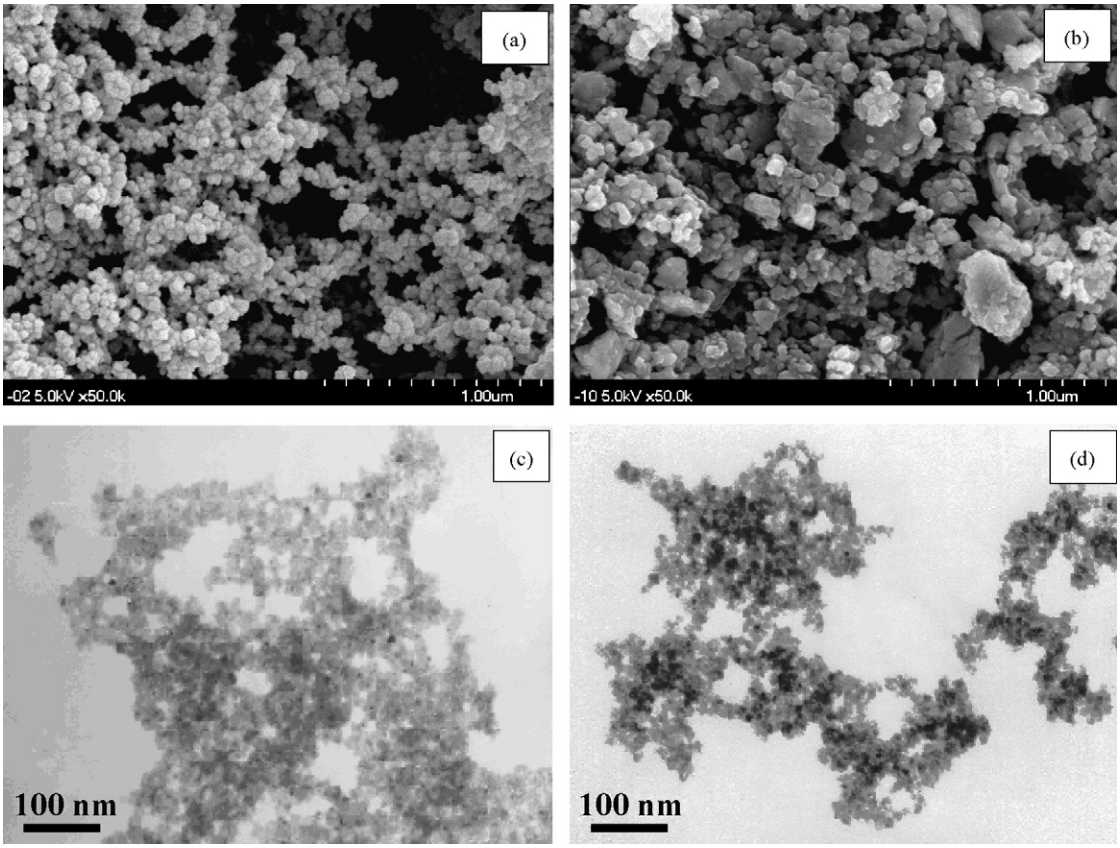

Fig. 4. FE-SEM and TEM microphotos of fresh (a) and (c) and used (b) and (d) of 15 wt.% NiO/Al_2O_3 catalyst, respectively used for waste MO catalytic gasification processes at T = 900 K and 1 atm.

nickel nanoparticles are well dispersed in the microstructures of Al_2O_3 supporter and the particle size is confirmed. Furthermore, FE-SEM or TEM analysis reveals that the nickel nanoparticles are highly dispersed on the surface of Al_2O_3 supporter. The size of the NiO nanoparticles is a very important factor as to determine the activity of the catalyst. Significant amount of NiO reduced to metallic Ni tested after gasification reaction is shown in Fig. 4(b) and (d), respectively. A few darker spot suggested that the reduced Ni concentrations occurred in certain areas with the particle size around 25–35 nm. The above results suggested that the temperature has a significant effect for the crystal migration behavior to increase the size of the catalyst. Generally, nickel nanoparticles are used to take participation for hydrogen formation in the higher reaction temperature [27]. XRD patterns of Ni, NiO and NiO/Al_2O_3 used and fresh catalyst are shown in Fig. 5. The XRD peaks of Ni, NiO and alumina become sharper at 44°, 55° and 76°, respectively is attributed to metallic nickel in Fig. 5(a) or (c). It is suggested that NiO is reduced to form Ni in the reaction. NiO catalyst peaks along with support materials are represented similar peak positions of Fig. 5(b) and (d), respectively. These attributed that fresh NiO/Al_2O_3 catalyst after involved into the reaction produced significant amount of metallic Ni on the catalyst surface.

In order to more thoroughly examine the nature of the Ni(0) or Ni(II) active species involved in catalytic gasification of waste MO, XANES and EXAFS spectra of Ni(0) or Ni(II) on Al_2O_3 in the waste MO catalytic gasification process were studied (Figs. 6 and 7). The XANES spectroscopy provides information of electronic configuration, stereochemistry and the oxidation states of nickel species being investigated [21–28]. In Fig. 6, the pre-edge XANES spectrum of NiO/Al_2O_3 catalysts exhibits a very weak absorbance feature for the 1s-to-3d transition, which is forbidden by the selection rule in the case of perfect octahedral symmetry [50]. The intensity of the 1s-to-4p_{xy} transition was proportional to the population of Ni(II) or Ni(0) on Al_2O_3 in the MO catalytic gasification process [51,52]. A shoulder at 8330–8333 eV and an intense feature at 8340–8350 eV were attributed to the 1s-to-4p_{xy} transition, that indicated the existence of Ni(II) species on Al_2O_3 in the MO catalytic gasification process [51–54]. However, the upshift of the edge energy and a very weak absorption feature for 1s-to-3d forbidden transition near the pre-edge also confirmed the observations. The XANES

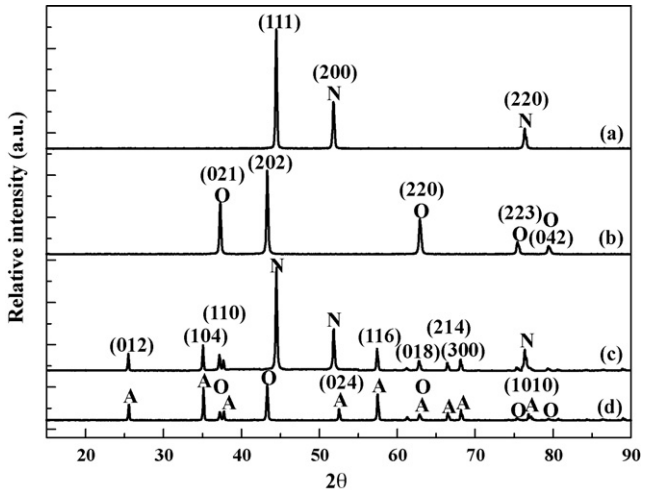

Fig. 5. XRD patterns of (a) Ni, (b) NiO standard, (c) used and (d) fresh 15 wt.% NiO/Al_2O_3 catalyst for waste MO catalytic gasification processes at 900 K and 1 atm (A: Al_2O_3; N: Ni; O: NiO).

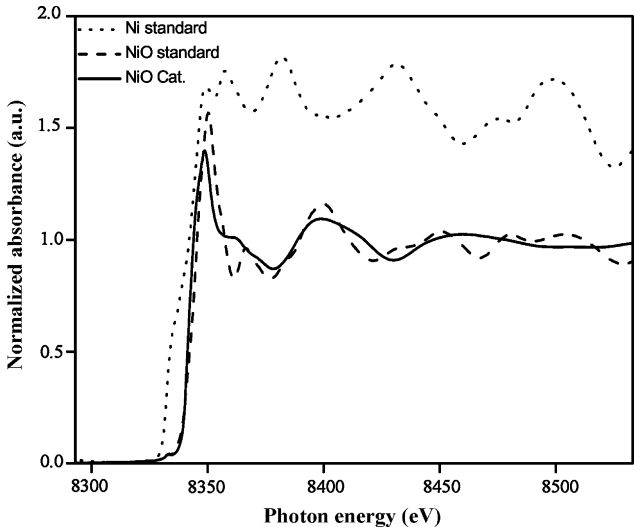

Fig. 6. XANES spectra of Ni or NiO standard, and nanophase 15 wt.% NiO/Al_2O_3 catalysts for waste MO catalytic gasification system at 900 K and 1 atm.

spectra worked particularly well in distinguishing of Ni(0) and Ni(II) species on Al_2O_3 support. In the waste MO catalytic gasification process, we found that most of the Ni(II) was reduced to Ni(0).

The main scientific issues concerning the chemical forms (or speciation) of active species ultimately depend on molecular-scale structure and properties. Basic understanding at this scale is essential for further understanding the catalytic behaviors of Ni or NiO on Al_2O_3 in the waste MO catalytic gasification process. Generally, Ni K-edge EXAFS spectroscopy can provide the information on the Ni atomic arrangement of catalysts in terms of bond distance, number and kind of near neighbors or thermal and static disorders [53]. The features of the XANES spectrum of NiO are significantly different from those of Ni foil, i.e., sharp absorption is observed at ca. 8350 eV for that of NiO [54]. An over 99% reliability of the Fourier-transformed EXAFS data fitting for NiO or Ni species on Al_2O_3 was obtained (Fig. 6). S.D. calculated from the averaged spectra was also determined. In all EXAFS data analyzed, the Debye–Waller factors ($\Delta\sigma^2$) were less than 0.02 Å^2. As shown in Fig. 7(a) and (b), central Ni atoms have a Ni–O and a Ni–Ni with bond distances of 2.04 ± 0.05 Å and 2.48 ± 0.05 Å, respectively on Al_2O_3 support. According with the Takenaka et al. [55] the peaks around at 2.04 ± 0.05 Å ascribed to the presence of Ni–O were not reduced easily by the reduction with hydrogen. In addition, the intensities of the peaks around 2.48 ± 0.05 Å were weak in the Fourier transforms of the EXAFS of Ni/Al_2O_3. These peaks would be due to Ni–Ni mainly. Therefore, it is likely that Ni species in Ni/Al_2O_3 were highly dispersed. Furthermore, a MO oxidation is occurred on the NiO/Al_2O_3 surface to produce metallic Ni species, could be the formation of tar/char in the gasification process. Since the complete MO combustion might be reduced into the tar/char content with the production of hydrogen-rich syngas, higher oxygen affinity of metallic nickel could be postulated as the formation of $NiAl_2O_3$. Therefore, EXAFS data revealed that the reduction in tar/char content prior to Ni catalysts was identified as a possible way to maintain the activity of the catalysts. Moreover, deactivation of the catalysts might occur as a result of carbon fouling and also of thermal sintering.

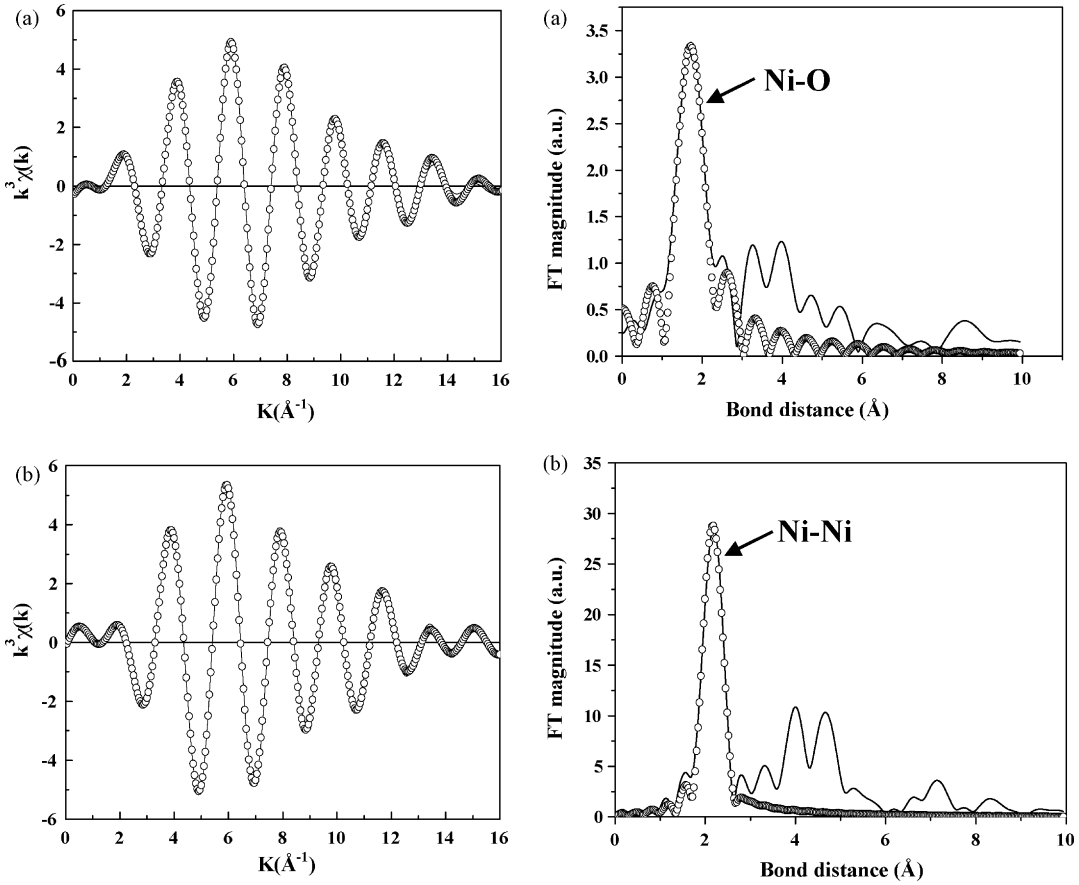

Fig. 7. Ni K-edge EXAFS oscillation $k^3\chi(k)$ and Fourier transform (FT) spectra of (a) fresh and (b) used 15 wt.% NiO/Al_2O_3 catalysts for waste MO catalytic gasification system at 900 K and 1 atm. The best fitting of the EXAFS spectra are expressed by the dotted lines.

3.3. Catalytic gasification mechanism and purification of syngas

The most promising option to generate hydrogen from waste MO (C_nH_{2n+2}) is the catalytic conversion included with n (where as, n is consisting with different hydrocarbon such as aliphatics or paraffin, olefin, etc.) [56,57]. In the catalytic gasification process, the waste MO is decomposed on the nickel catalyst surface to produces a complex consisting of the decomposed organic compound according to reaction (1):

$$C_nH_{2n+2} + NiO \rightarrow C_nH_{n+1}{-}Ni + (n/2)H_2 + H_2O \quad (1)$$

$$C_nH_{n+1}{-}Ni + (1-x)NiO \rightarrow nCO + ((n+1)/2) \quad H_2 + Ni \quad (2)$$

$$Ni + H_2O \rightarrow NiO + H_2 \quad (3)$$

$$C + O_2 \rightarrow CO_2 \quad (4)$$

$$C + H_2O \rightarrow CO + H_2 \quad (5)$$

$$CO + H_2O \rightarrow CO_2 + H_2 \quad (6)$$

$$C_nH_{2n+2} + nCO_2 \rightarrow nCO + (n+1)H_2 \quad (7)$$

Overall reaction (not stoichiometric):

$$MO + O_2 + H_2O \rightarrow CO + H_2$$

The complex intermediate molecule further reacts with NiO (where as $(1-x)$ is the remaining amount of the catalyst) to produce CO, H_2 or metallic Ni as proposed by reaction (2) and is observed through XRD and EXAFS spectra. Water oxidizes metallic nickel and produces NiO and H_2 by reaction (3). The steam reforming of the MO may also generate carbon (coke) on the catalyst surface as an unwanted side effect. Carbon formation increased with unsaturation and molecular weight. Mechanisms of carbon formation as well as methods for its minimization on the catalyst surface have been proposed previously. There were two different method were used based on the enhancing steam adsorption on the catalyst and another one is modifying the surface reactions with the presence of other metals [11]. However, it is well known that Ni-based catalysts are more effective for less carbon depositing [14,24–34]. Oxygen and carbon in waste MO reacted in a highly exothermic manner that supplying heat to keep the endothermic reaction going to give H_2 production as reactions (4) and (5). In addition, CO shift reaction (6) (exothermic and rapid reaction ($\Delta H = -8.093$ kcal mol^{-1} at 900 K)) [56] was also limited by the amount of water steam present in the catalytic gasifier. Reactions (1)–(5) were the main reactions producing H_2 and CO. The net catalytic gasification reaction was produced H_2 prominently. Furthermore, MO is gasified to CO and H_2 by reaction (2), where as complex organic compound on to the metallic surface decomposed to metallic Ni, thermodynamically would be required higher energy ($\Delta H > 0$) for completing this reaction [57,58]. This result suggested that reaction (2) is the slowest reaction and hence rate-controlling step of the overall gasification reaction also significant approaches is observed via physical characterization of the NiO/Al_2O_3 through this study. The elimination of the CO_2 is achieved by the reforming of the hydrocarbons generally obtained from Eq. (7) in the syngas. In this study, two typical infrared spectra for the syngas generated from waste MO catalytic and non-catalytic gasification were shown in Fig. 3(a) and (b), respectively. As expected, the stretching band of CO, CO_2 and H_2O gases were observed at 2005–2250 cm^{-1}, 2250–2370 cm^{-1} and 3700–3950 cm^{-1} (or 1500–1800) cm^{-1}, respectively, obviously indicating that the catalytic gasification reactions have occurred. In addition, in the presence of the catalyst MO has higher gasification on CO production then without catalyst was found in Fig. 3(b). Therefore the intensity of the CO formation at 2005–2250 cm^{-1} is significantly lower, implying an incomplete reaction involved in the complicated non-catalytic gasification of waste MO with strong bonding of aliphatics or paraffins. This result may be caused mainly by the high-molecular-weight components in waste MOs, which were not completely destroyed at a lower gasification temperature of 900 K without catalysts. Since the composition of waste MO is very complicated, the catalytic gasification of waste MO may produce some additional by-products. Among them, sulfur in the waste MO was primarily react with Ni catalyst to form NiS and then converted into H_2S, which was easily removed from the syngas by conventional cleanup methods. Since the Ni–O bonding is weaker than Ni–S bonding, hydrogen sulfur is then oxidized with water to sulfur dioxide with formation of hydrogen ($H_2S + 2H_2O \rightleftharpoons SO_2 + 3H_2$) [59,60]. Nitrogen was converted into N_2, with minor traces or no detected of NH_3, which might readily be dissolved in the process water and neutralized with the acidic feed components such as chlorides. Finally, little NO_x or SO_x may be formed due to the chemically reducing atmosphere in the MO catalytic gasifier [38].

3.4. Basic design of catalytic gasification process

In this work, experimental data obtained from the lab-scale waste MO catalytic gasification system can be used as the basis for the scale-up of this technology. In that follows, some simulation calculations and parameter evaluations were given for this system with the reaction or equilibrium equations using the EXCEL software. The principal operational units in the united gasification of simulated waste MO include a gasifier section (including a CO shift section), H_2 purification section (pressure swing adsorption (PSA) and Pd membrane purifier), and the final PEMFC are represented in Fig. 8 [61]. The particulate free and saturated syngas are obtained from the simulated waste MO streams gasification unit. This unit employed one or two fixed catalytic beds to convert CO and steam into CO_2 and H_2. The water gas shift reaction can be simply expressed by the following equation: $CO + H_2O$ (CO shift conversion) $\rightarrow CO_2 + H_2$ ($\Delta H = -8.093$ kcal mol^{-1} at 900 K) [56]. Since the reaction was highly exothermic, a conventional heat-recovery exchanger could be used to generate medium-pressure steam for export or captive consumption. The effluent gas from the CO shift unit was then fed to a PSA unit for H_2 purification with Pd membranes. Adsorbent beds at high pressure removed the impurities and a high-purity (>99.99%) H_2 stream was effectively produced shown in Fig. 8 [61]. The adsorbed impurities were then concentrated and removed at low pressure in the form of a reject-gas stream. Depending on the feedback characteristics, the reject gas can be partially recycled to the process, or used in the refinery or petrochemical industries. As shown in Fig. 8, the material and energy balances of the waste MO catalytic gasification process may provide the essential information about the operational condition in the system and determine if further developments would be warranted. The process consists of a waste MO feed system, a downdraft type gasifier, an ash discharge system, a coke/tar/slag or water adsorber, an internal combustion engine for power generation, CO/H_2 separator, hydrogen purifier, and an integrated PEMFC. Simulated data indicate that in order to generate a 100 kW electric power, approximately 200 kg h^{-1} of waste MO would be catalytically gasified at 760–900 K and 46.2 atm with the reactor volume 0.27 m^3. The global material balance for this catalytic gasification process was >95%. An illustration of the process design concept for the treatment of the simulated waste MO with catalytic gasification system from Fig. 8 is shown in Table 4. In the simulated pilot-scale continuous operation of downdraft-type waste MO catalytic

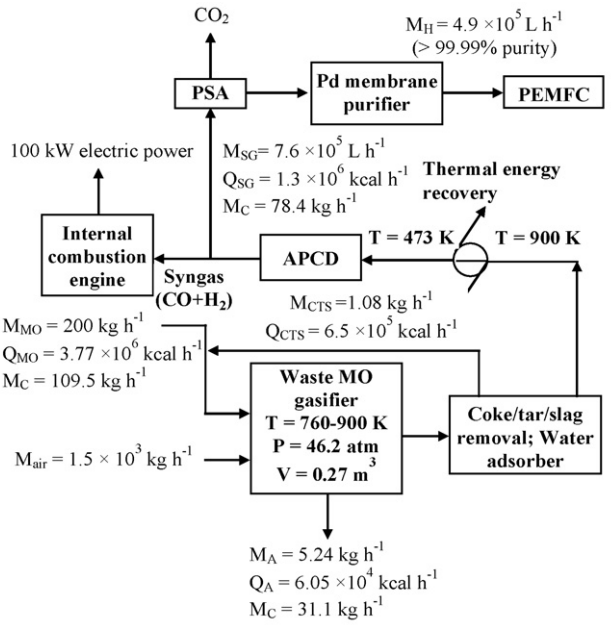

Design basis: 100 kW h^{-1} of electric power generated from waste motor oil catalytic gasification.

Note: 1. Eight hours operation per day with preheating the catalytic gasifier by natural gas;
2. Assuming tar or slag was produced from 0.5% unconversion carbon of MO catalytic gasification;
3. Assuming O/C mole ratio = 1.10-1.30;
4. A, C, MO, SG, H, and CTS denote the mass of ashes, carbon, waste motor oil, syngas, hydrogen, and coke/tar/slag, respectively.
5. PSA and APCD denote "pressure swing adsorption and air pollution control device, respectively.

Fig. 8. Material and energy balances of a pilot-scale waste MO catalytic gasification process with hydrogen generation in an integrated PEMFC.

gasification system included with individual units to be as stand-alone as possible in moderate-to-high level of automation was carried out with temperatures were much higher than 700 K and the main products were CO and H_2. In addition, the pressure of waste MO catalytic gasifier was usually based on the pressure required for the delivery of the ultimate product (CO or H_2) to its end use (for instance, an integrated PEMFC or the refinery hydrogen header pressure) and purification is carried out through PSA to separate CO_2. Generally, operating pressures in the commercial biomass or coal non-catalytic gasification processes are ranged from 50 atm to 80 atm [6,40–44]. It is noteworthy that a commercial catalytic gasifier often operates at mid-term temperatures or pressures and a well-mixed gaseous environment in which the partial oxidation reactions take place.

In order to optimize the operation conditions of simulated MO catalytic gasification process, shift temperatures, O/C mole ratios, and the amounts of waste MOs were moderately adjusted. Table 5 and Fig. 9 provide a summary of results from the simulated MO catalytic gasification process. Specific oxygen consumption (SOC) and cold gas efficiency values of MO catalytic gasification process increased and decreased, respectively, with an increase of O/C ratio that also enhanced the MO catalytic gasification rate shown in Fig. 9(a). As shown in Table 5, over 85% of CO and H_2 were obtained from the catalytic gasification of waste MO at 900 K and 46.2 atm in a 0.27 m^3 catalytic gasifier. It should be noted that the process, in terms of heat requirements, could be self-sustaining during the catalytic gasification process. In addition, syngas may have harmful contents such as trace chlorine or sulfur, the conversions of waste MO to fuel gas reformate, hydrogen production, and final processing to make it suitable for an integrated fuel processor and power generation system. The MO fed as feedstock to the catalytic gasifier without pretreatment and the generated pure hydrogen streams were designed to be recycled for captive consumption. Since catalytic gasification of the waste MO produced virtually no

Table 5
Composition of syngas obtained from a simulated waste motor oil catalytic gasification process (unit: mol%)

CO	32.7
CO_2	12.8
H_2	53.3
N_2	0.5
CH_4	0.5
H_2S	<0.01
COS	<0.01
Cold gas efficiency	77–84%
Heat recovery	8.35×10^5 kcal h^{-1}

Table 4
Design basis of a 10-TPD catalytic gasification system of waste MO for an integrated PEMFC

Design philosophy	
Downdraft-type catalytic gasification system	
Continuous operation	
Individual units to be as stand-alone as possible	
Moderate-to-high level of automation	
Major design parameters	
Feeds—Liquid waste MO without pretreatment	
Air and/or steam	
Operational conditions	
Feed rate	10-TPD
Volume of gasifier	0.27 m^3
Heat loss	5.56×10^3 kcal h^{-1}
Unconversion carbon	0.5%
O/C	1.1–1.3 atom/atom
T, P	900 K, 46.2 atm
Desired power output	100 kW
Ultimate product fate	
Ash	Reclaimed in carbon steel manufacturing
Syngas	Fuel gas (CO + H_2 = 86%, dry basis)
Syngas	Generation of electric power
CO	Shift to hydrogen
H_2	Recycling (supply for a PEMFC or others)

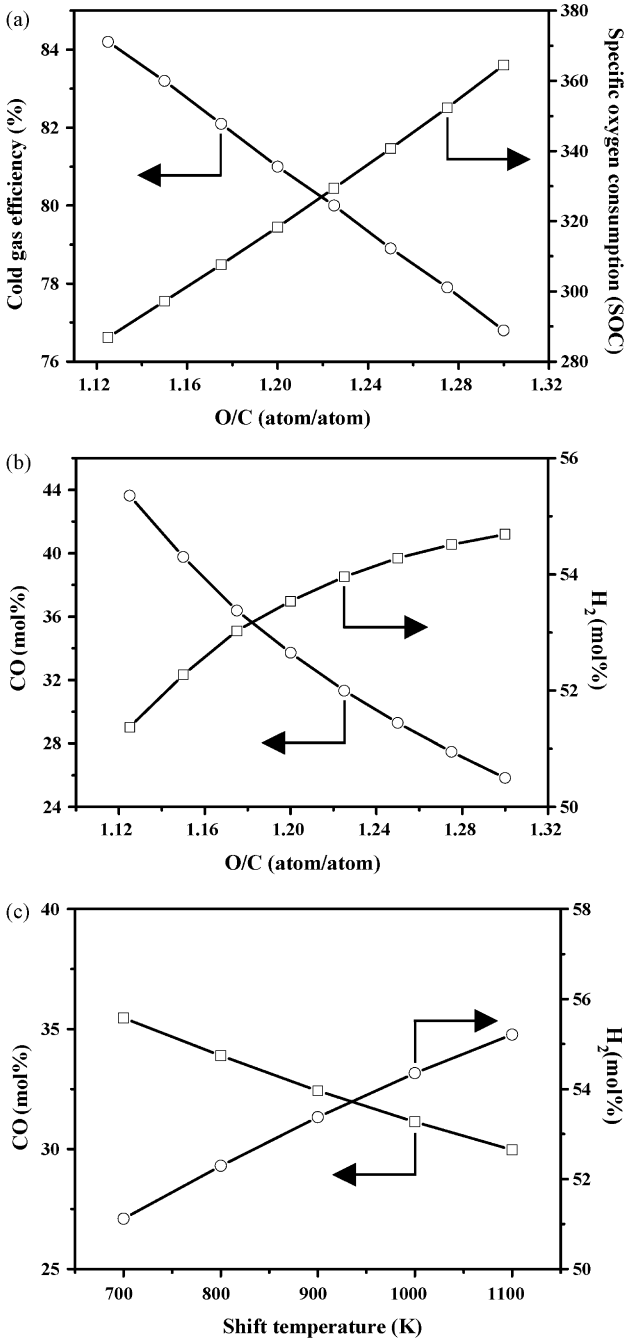

Fig. 9. Relationship of (a) cold gas efficiency (CGE) or specific oxygen consumption (SOC) at different shift temperatures, CO or H_2 molar percentage in (b) different O/C atom ratio, and (c) different shift temperatures for a 10-TPD pilot-scale waste MO catalytic gasification process.

sulfur or nitrogen oxides emissions, water usage was also small. Moreover, in addition to the syngas generation, approximately 8.35×10^5 kcal h^{-1} of thermal energy may be recovered from the catalytic gasification process also shown in Table 5. The CGE may reach 77–84% when the catalytic gasifier process is operated at the O/C ratios between 1.13 and 1.30. In addition, the MO catalytic gasification reaction ($MO + O_2 + H_2O \rightarrow CO + H_2$) and the CO water shift reaction ($CO + H_2O \rightarrow CO_2 + H_2$) were also influenced by both the O/C ratio and shift temperature of the catalytic gasifier. Fig. 9(b) indicated that amounts of CO decreased and H_2 increased, with an increase of O/C ratio. On the other hand, an increase of O/C ratio caused an increase of CO_2 that was limited by the CO shift reaction. According to Fig. 9(c), the reaction rate of the highly exothermic and rapid water-shift reaction are decreased with increasing shift temperatures from 700 K to 1100 K, indicating that an increase in the reaction temperature favored the formation of H_2 and decomposition of the CO [26–28,30]. Increasing with the temperature influenced the O/C ratio from Fig. 9(b). Therefore, equilibrium is not reached for the formation of H_2 for an integrated PEMFC.

Table 6
Economic benefits[a] of a 10-TPD[b] or 20-TPD retrofitted catalytic gasification process for treatment of the waste MO

	Cash flow (×US$ 10,000)					
	10-TPD			20-TPD		
	1st year	2nd year	3rd year	1st year	2nd year	3rd year
Sales	19.68	23.75	26.19	31.58	37.22	40.49
Production cost[c]	16.47	19.41	20.67	27.36	30.98	32.91
Cash inflow	3.21	4.34	5.52	4.22	6.24	7.58
Payback (year)		2.6		2.1		

Notes: initial capital investments of 10-TPD and 20-TPD are 10.29 and 11.08 (×US$ 10,000), respectively include land, machineries and freight, erection and installation, insurance, etc.
[a] Tipping fee for treatment of waste MO = US$ 190–220 ton^{-1}.
[b] The pilot-plant catalytic gasification process was operated 24 h per day.
[c] Production cost includes raw material, labor, manufacturing overheads, depreciation, non-operating expenses, etc.

3.5. Cost/benefit analysis

As mentioned earlier, in the united catalytic gasification of waste MO that are easily collected and transported to a gasification treatment center, individual APCD can be eliminated for higher economic benefit. This permits considerable flexibility in adapting to existing waste MO collection stations as well as in adapting to new installations where high-purity hydrogen is needed at high pressure. On the other hand, it was found that developing a lower-temperature catalytic gasification process of waste MO for hydrogen recovery could save 28–35% of capital investment over conventional hydrogen supply processes (steam reforming). Moreover, if 24-h workday was taken, a 20-TPD catalytic gasification process had better economic benefits than a 10-TPD one shown in Table 6. Due to the use of a fully automatic control scheme in this 10-TPD pilot plant of MO catalytic gasification, only two operators per shift were required in handling of MO samples feed, data processing (local readout), and computer controlling. Currently, the tipping fee for the treatment of waste MO was about US$ 190–220 ton^{-1} in Taiwan. Therefore, anticipated payback for a waste MO catalytic gasification plant with a capacity of 10- or 20-TPD was approximately 2.6 or 2.1 years, respectively [62].

4. Conclusions

The feasibility for the waste MO catalytic gasification was investigated. Based on the catalytic gasification experimental data obtained from the lab-scale downdraft-type reaction system, the primary engineering design for a pilot plant of the waste MO catalytic gasification process was also accomplished. It appears that approximately 200 kg h^{-1} of waste MO would be gasified to generate 100 kW electric power. A 1-TPD pilot plant is currently under construction in fuel cell center of Yuan Ze University, Taiwan to prove technical and economic viability of the MO catalytic gasification process concept. In the waste MO catalytic gasification process, most of the Ni(II) reduced to Ni(0) was found by XANES spectra. The EXAFS data also showed that the central Ni atoms have

a Ni–O and a Ni–Ni with bond distances of 2.04 ± 0.05 Å and 2.48 ± 0.05 Å, respectively on Al_2O_3 support. Thus, the peaks around at 2.04 ± 0.05 Å ascribed to the presence of Ni–O bonding was not reduced easily by the reduction with hydrogen. In addition, the intensities of the peaks around 2.48 ± 0.05 Å were weak in the Fourier transforms of the EXAFS of Ni/Al_2O_3. These peaks would be due to Ni–Ni bonding mainly. Therefore, it is likely that Ni species in Ni/Al_2O_3 were highly dispersed. So, a complete oxidation of MO occurred to form Ni on the catalyst surface and start to generate the production of hydrogen. The material and energy balances of the 10-TPD gasifier system pointed out that >85% (dry basis) of H_2 and CO were generated at 900 K and 46.2 atm, and in addition to the hydrogen generation, approximately 8.35×10^5 kcal h^{-1} of thermal energy may be recovered. Cost/benefit analysis showed that the number of years of payback for 10- and 20-TPD MO catalytic gasification processes were about 2.6 and 2.1, respectively. In addition, the catalytic gasification of MO to syngas, production of high-purity hydrogen, and final processing to make it suitable for the integrated fuel cell power generation system.

Acknowledgement

The financial supports of National Science Council (Contract No.: NSC-93-2211-E-155-001) of Taiwan, ROC are gratefully acknowledged.

References

[1] ROC EPA, A planning report for the recycling strategies of waste motor oils, EPA–95-09-405, EPA, ROC, 2006.
[2] G.V. Rossum, S.R.A. Kersten, W.P.M.V. Swaaij, Ind. Eng. Chem. Res. 46 (2007) 3959–3967.
[3] K.S. Lin, C.K. Lee, J. Practice Period Hazard. Toxic Radioact. Waste Manage. 10 (2006) 150–155.
[4] P. García-Ibañez, A. Cabanillas, J.M. Sánchez, Biomass Bioenergy 27 (2004) 183–194.
[5] M.C. Ramos, A.I. Navascués, L. García, R. Bilbao, Ind. Eng. Chem. Res. 46 (2007) 2399–2406.
[6] K.S. Lin, H.P. Wang, C.J. Lin, C.I. Juch, Fuel Process. Technol. 55 (1998) 185–192.
[7] T. Davidian, N. Guilhaume, E. Iojoiu, H. Provendier, C. Mirodatos, Appl. Catal. B: Environ. 73 (2007) 116–127.
[8] P.N. Kechagiopoulos, S.S. Voutetakis, A.A. Lemonidou, I.A. Vasalos, Energy Fuels 20 (2006) 2155–2163.
[9] K.A. Simonsen, L.F. O'Keefe, W.F. Fong, Oil Gas J. 56 (1993) 45–48.
[10] F. Jahnke, TAPPI J. 82 (1999) 49–53.
[11] Z. Wang, Y. Pan, T. Dong, X. Zhu, T. Kan, L. Yuan, Y. Torimoto, M. Sadakata, Q. Li, Appl. Catal. A: Gen. 320 (2007) 24–34.
[12] M.F. Bleeker, S.R.A. Kersten, H.J. Veringa, Catal. Today 127 (2007) 278–290.
[13] S. Panigrahi, A.K. Dalai, S.T. Chaudhari, N.N. Bakhshi, Energy Fuels 17 (2003) 637–642.
[14] A. Sharma, H. Nakagawa, K. Miura, Fuel 85 (2006) 179–184.
[15] L.I. Darvell, K. Heiskanen, J.M. Jones, A.B. Ross, P. Simell, A. Williams, Catal. Today 81 (2003) 681–692.
[16] M.A. Caballero, J. Corella, M.P. Aznar, J. Gil, Ind. Eng. Chem. Res. 39 (2000) 1143–1154.
[17] D. Świerczyński, C. Courson, L. Bedel, A. Kiennemann, J. Guille, Chem. Mater. 18 (2006) 4025–4032.
[18] M. Benito, S. García, P.F. Aparicio, L.G. Serrano, L. Daza, J. Power Sources 169 (2007) 177–183.
[19] K. Sato, K. Fujimoto, Catal. Commun. 8 (2007) 1697–1701.
[20] T. Kimura, T. Miyazawa, J. Nishikawa, S. Kado, K. Okumura, T. Miyao, S. Naito, K. Kunimori, K. Tomishige, Appl. Catal. B: Environ. 68 (2006) 160–170.
[21] A. Sharma, I. Saito, H. Nakagawa, K. Miura, Fuel 86 (2007) 915–920.
[22] B. Li, K. Maruyama, M. Nurunnabi, K. Kunimori, K. Tomishige, Ind. Eng. Chem. Res. 44 (2005) 485–494.
[23] M. Inaba, K. Murata, M. Saito, I. Takahara, Energy Fuels 20 (2006) 432–438.
[24] L. Garcia, A. Benedicto, E. Romeo, M.L. Salvador, J. Arauzo, R. Bilbao, Energy Fuels 16 (2002) 1222–1230.
[25] C. Courson, L. Udron, D. Świerczyński, C. Petit, A. Kiennemann, Catal. Today 76 (2002) 75–86.
[26] L. Wang, K. Murata, Y. Matsumura, M. Inaba, Energy Fuels 20 (2006) 1377–1381.
[27] K. Matsuoka, T. Shinbori, K. Kuramoto, T. Nanba, A. Morita, H. Hatano, Y. Suzuki, Energy Fuels 20 (2006) 1315–1320.
[28] C. Courson, E. Makaga, C. Petit, A. Kiennemann, Catal. Today 63 (2000) 427–437.
[29] K. Tomishige, T. Kimura, J. Nishikawa, T. Miyazawa, K. Kunimori, Catal. Commun. 8 (2007) 1074–1079.
[30] T. Wang, J. Chang, X. Cui, Q. Zhang, Y. Fu, Fuel Process. Technol. 87 (2006) 421–428.
[31] D. Sutton, B. Kelleher, J.R.H. Ross, Fuel Process. Technol. 73 (2001) 155–173.
[32] R. Martínez, E. Romero, L. García, R. Bilbao, Fuel Process. Technol. 85 (2003) 201–214.
[33] A. Sharma, H. Nakagawa, K. Miura, Fuel 85 (2006) 2396–2401.
[34] S.C. Tsang, J.B. Claridge, M.L.H. Green, Catal. Today 23 (1995) 3–15.
[35] Y. Zhang, G. Xiong, S. Sheng, W. Yang, Catal. Today 63 (2000) 517–522.
[36] C. Cellier, B. Blangy, C. Mateos-Pedrero, P. Ruiz, Catal. Today 112 (2006) 112–116.
[37] F. Patcas, F.C. Patcas, Catal. Today 117 (2006) 253–258.
[38] Z.A. El-Rub, E.A. Bramer, G. Brem, Ind. Eng. Chem. Res. 43 (2004) 6911–6919.
[39] P. Forzatti, L. Lietti, Catal. Today 52 (1999) 165–181.
[40] G. Centi, S. Perathoner, Catal. Today 77 (2003) 287–297.
[41] P. Ji, W. Feng, H.J.V. Kooi, J.D.S. Arons, Ind. Eng. Chem. Res. 43 (2004) 2005–2016.
[42] M.P. Aznar, M.A. Caballero, J. Corella, G. Molina, J.M. Toledo, Energy Fuels 20 (2006) 1305–1309.
[43] S.M. Swami, M.A. Abraham, Energy Fuels 20 (2006) 2616–2622.
[44] L. Ma, H. Verelst, G.V. Baron, Catal. Today 105 (2005) 729–734.
[45] Z.S. Petrović, Z.Z. Zavargo, J. Appl. Polym. Sci. 32 (1986) 4353–4367.
[46] H.L. Friedman, J. Polym. Sci., Part C 6 (1964) 183–195.
[47] F.W. Lytle, J. Synchrotron Rad. 6 (1999) 123–134.
[48] S.A. Qian, C.F. Li, P.Z. Zhang, Fuel 63 (1984) 268–275.
[49] V. Srica, J. Muhl, M. Jednacak, A. Duric, Fuel 72 (1993) 775–778.
[50] M.J. Paek, T.W. Kim, S.J. Hwang, J. Phys. Chem. Solids 69 (2008) 1444–1446.
[51] F. Farges, G.E. Brown Jr., P.E. Petit, M. Munoz, Geochim. Coscochim. Acta 65 (2001) 1665–1678.
[52] L. Galoisy, L. Cormier, G. Galas, V. Briois, J. Non-cryst. Solids 293–295 (2001) 105–111.
[53] R.F.D. Souza, L.C. Simon, M.D.C.M. Alves, J. Catal. 214 (2003) 165–168.
[54] S. Takenaka, E. Kato, Y. Tomikubo, K. Otsuka, J. Catal. 219 (2003) 176–185.
[55] S. Takenaka, H. Ogihara, I. Yamanaka, K. Otsuka, Appl. Catal. A: Gen. 217 (2001) 101–110.
[56] J.A.C. Dias, J.M. Assaf, J. Power Sources 137 (2004) 264–268.
[57] G. Egloff, E.F. Nelson, J.C. Morrell, Ind. Eng. Chem. 29 (1937) 555–559.
[58] D. Gourgouillon, L. Schrive, S. Sarrade, G.M. Rios, Environ. Sci. Technol. 34 (2000) 3469–3473.
[59] J. Srinakruang, K. Sato, T. Vitidsant, K. Fujimoto, Fuel 85 (2006) 2419–2426.
[60] C. Lombard, S.L. Doze, E. Marencak, P.M. Marquaire, D.L. Noc, G. Bertrand, F. Lapicque, Int. J. Hydrogen Energy 31 (2006) 437–440.
[61] G. Chiappetta, G. Clarizia, E. Drioli, Chem. Eng. J. 124 (2006) 29–40.
[62] R. Chaney, L.V. Bibber, Beluga Coal Gasification Feasibility Study, DOE/NETL-2006/1248, Phase I, Final Report for Subtask 41817.333.01.01 (July 2006).